JOURNAL OF MAGNETIC RESONANCE **125,** 216–219 (1997)
ARTICLE NO. MN961101

Ultra-High-Resolved HSQC Spectra of Multiple-^{13}C-Labeled Biofluids

WIELAND WILLKER, ULRICH FLÖGEL, AND DIETER LEIBFRITZ

Institut für Organische Chemie, Fachbereich 2, Universität Bremen, 28334 Bremen, Germany

Received December 17, 1996

The NMR analysis of cell extracts and culture media from cells fed with multiple-^{13}C-labeled substrates such as [U-$^{13}C_6$]glucose gives access to various aspects of cellular metabolism. ^{13}C NMR allows the simultaneous identification of individual ^{13}C isotopomers in order to distinguish different metabolic pathways. These measurements are commonly carried out with 1D carbon spectroscopy (*1–6*). The advantage of this method is that all labeled carbons are detected in one spectrum with very high spectral resolution. The disadvantages, however, are the low sensitivity, the signal superpositions, and the need to assign unknown resonances based on chemical shifts only. In contrast, 2D inverse H,C spectroscopy offers better signal separation, very high sensitivity, and tools to confirm the assignment (*7*). A drawback is the low resolution in the carbon dimension. Especially at high field (600/800 MHz), it is almost impossible to resolve C–C couplings with an acceptable number of t_1 increments in a nonselective HSQC experiment. To overcome this limitation, we have recently proposed a region-selective HSQC (*8*). Here we present an improved version and optimum combination with *J* scaling and constant-time evolution. Applications to a multilabeled cell extract of F98 glioma cells are shown.

All experiments were performed on a Bruker DRX 600 MHz spectrometer. A 5 mm, H,C,N, inverse triple-resonance probe with shielded gradients was used. Gradients were shaped by a waveform generator and amplified by a Bruker Acustar amplifier. Sinusoidal *z* gradients of duration 1 ms and recovery time 100 μs have been used for echo/antiecho gradient selection. Gradient fine adjustment (40:10.08) has been performed to get optimum intensity. Low-power adiabatic composite-pulse decoupling with WURST (*9*) has been used. A Gaussian 180° pulse of length 1 ms was used to excite a range of 15 ppm in F_1(^{13}C). The selective HSQC experiments were acquired with 512 or 1024 t_1 increments, for a spectral width of 15 ppm, to give a digital resolution in the carbon dimension of 4 or 2 Hz/pt. An acquisition time of 285 ms has been used to acquire a spectral width of 3 ppm in the proton dimension using digital quadrature detection. For the carbon spectra, an H,C dual probe was used with acquisition time 0.9 s and repetition time 2 s. This affords a digital resolution of 0.55 Hz/pt. The spectra were multiplied by an exponential weighting function, giving an additional line broadening of 2 Hz.

F98 glioma cells were grown to confluency in 15 cm culture dishes in a humidified atmosphere of 10% CO_2 in air at 37°C in DMEM, supplemented with 5% FCS and penicillin/streptomycin (100 units/ml). For cell extracts, approximately 10^8 cells obtained from four culture dishes were incubated for 24 h in DMEM medium containing 8 m*M* [U-$^{13}C_6$]glucose. All samples were adjusted to pH values of 7–8.

Sensitivity-improved HSQC with gradient echo/antiecho selection is used for optimum sensitivity (*10, 11*). There are several possibilities for introducing a selective pulse into this pulse sequence. The sequence in Fig. 1a replaces the carbon 90° excitation pulse with a G4 Gaussian pulse cascade (*12*), and the sequence in Fig. 1b replaces the 180° pulse in the first INEPT step with a Gaussian 180° pulse. The pulse sequence in Fig. 1a is similar to the pulse sequence presented in (*8*), but is now combined with sensitivity improvement. The advantage of the new pulse sequence shown in Fig. 1b is that it is of the same length as the nonselective HSQC with a signal intensity of approximately 120% compared to sequence 1a. However, the advantage of sequence 1a is an almost rectangular excitation profile of the G4 Gaussian pulse cascade. Sequence 1b requires a symmetrical pulse. We used a Gaussian 180° pulse, but other symmetrical pulses like hyperbolic secant are also possible.

A useful feature of 2D spectroscopy is *J* scaling (*13*). The evolution of the chemical shift can be manipulated by inserting 180° pulses into the evolution time t_1. In our case, an upscaling of the ^{13}C–^{13}C coupling constants was required. This can be obtained by introducing an additional 180° carbon pulse and adding several incremented d_0 delays (Fig. 1c). J_{CC} evolution occurs during the full t_1 period, whereas ^{13}C chemical shift evolves only during the last two d_0 delays. This version scales up the ^{13}C–^{13}C coupling by a factor of 3. Additional d_0 delays cause an even greater upscaling but may cause signal loss due to relaxation. *J* scaling offers the opportunity to unravel superimposed lines by utilizing variable line splitting. This holds, for example, if one element of a multiplet pattern is superimposed on a singlet signal of a monolabeled ^{13}C isotopomer.

1090-7807/97 $25.00

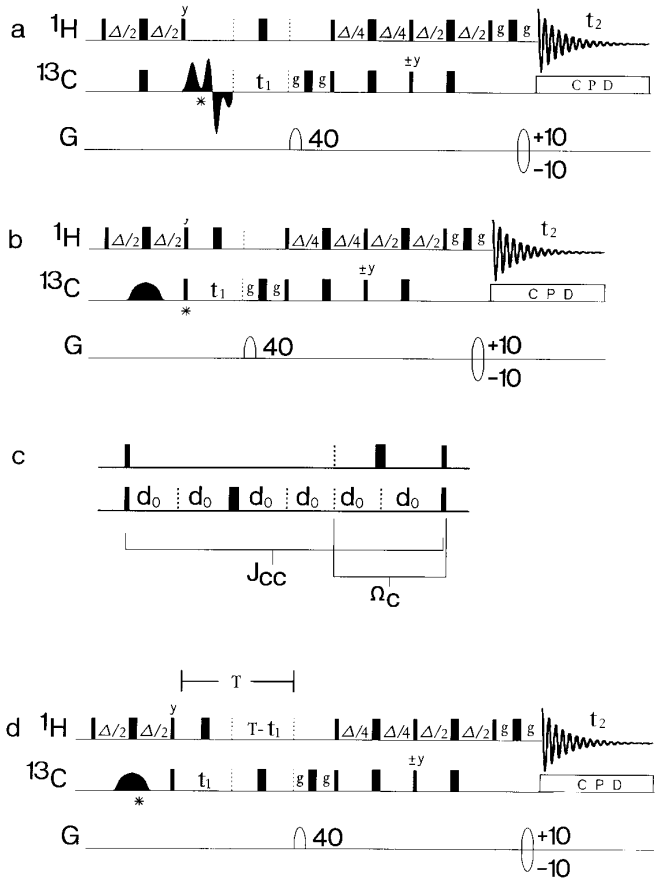

FIG. 1. Pulse sequences. (a) The region-selective sensitivity-improved HSQC with a selective G4 Gaussian pulse cascade replacing the first carbon 90° hard pulse. (b) The same sequence but with a selective 180° Gaussian pulse replacing the first carbon 180° hard pulse. (c) The t_1 time element for J scaling. (d) The region-selective CT-HSQC. $\Delta = (2*{}^1J_{CH})^{-1}$, * = TPPI, g = gradient time = 1.1 ms, d_0 = incremented delay in t_1, T = constant-time delay. The gradients select the single-quantum echo (40/−10) and the antiecho (40/+10).

The region-selective CT-HSQC is depicted in Fig. 1d. The principles of the pulse sequence and the $^{13}C(^{13}C)_n$ multiplicity editing have been discussed previously (*8*). The correct choice of the constant time T, which controls the coherence-transfer factor, can be difficult if the mixture contains compounds with different and a priori unknown labeling patterns. The intensity of a carbon signal as a function of T is given by $\cos^n(\pi J_{CC}T)$ with the carbon–carbon multiplicity $n = {}^{13}C-(^{13}C)_n$. For example, the F98 glioma cell extract shows a doublet of 51 Hz and a doublet of doublets of 51/34 Hz for glutamate C4, whereas a doublet of 34 Hz and a doublet of doublets of 34/34 Hz are found for C3. Figure 2 shows the different intensity functions for these isotopomers. Fortunately, an optimum T value is found at 60 ms. After this constant time T, all carbons with a large (51 Hz) or a combination of large and small (34 Hz) coupling constants give negative signals, while carbons with small coupling constants only give positive signals. To predict the optimum time T, one must consider all possible coupling patterns in order to calculate the expectable evolution curves.

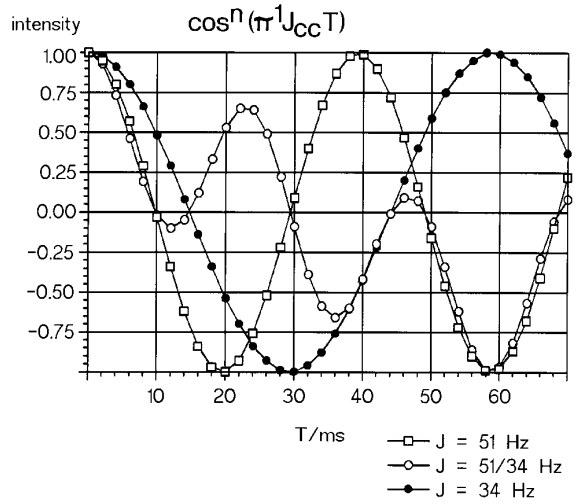

FIG. 2. Intensity evolution of signals with different $^1J_{CC}$ coupling constants as a function of T. Open squares represent a signal with $^1J_{CC}$ = 51 Hz coupling, open circles represent a signal with two different coupling constants ($^1J_{CC}$ = 51 and 34 Hz) and filled circles represent a signal with only $^1J_{CC}$ = 34 Hz coupling. The optimum T value is 60 ms for these cases.

All applications presented are performed on a PCA extract of F98 glioma cells fed for 24 h with [U-$^{13}C_6$]glucose. Figure 3 shows the signal obtained for proline C4. The multiplet represents a superposition of signals from two different isotopomers. It consists of a doublet [^1J(C4–C5) = 33.2 Hz] and a doublet of doublets [^1J(C4–C5) = 33.2 Hz and ^1J(C3–C4) = 30.4 Hz]. On the left, the 1D carbon spectrum is shown. Figure 3a is obtained with the region-selective HSQC of Fig. 1b. The spectral resolution of the 2D spectrum is the same as in the 1D carbon spectrum. Figure 3b is acquired with J scaling by a factor of 3. The true spectral resolution is the same as in the left spectrum (4 Hz/pt), but the virtual resolution is higher, because the two coupling

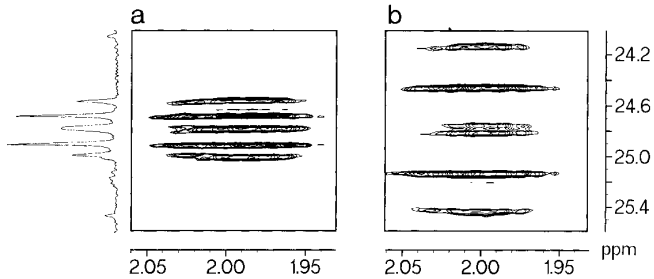

FIG. 3. Proline C4 signal of an F98 glioma PCA cell extract. On the left, the 1D carbon spectrum is shown: (a) obtained with pulse sequence of Fig. 1b and (b) obtained with pulse sequence of Fig. 1b combined with J scaling (Fig. 1c).

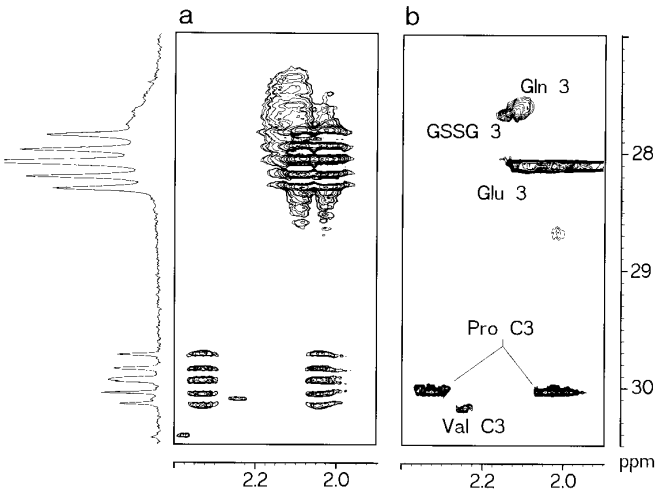

FIG. 4. Pro/Glx-C3 region of the F98 glioma PCA cell extract. The 1D carbon spectrum is shown on the left: (a) Obtained with pulse sequence Fig. 1b, (b) obtained with pulse sequence Fig. 1d, which is the constant-time version. (Gln = glutamine, GSSG = glutathione, Glu = glutamate, Pro = proline, Val = valine.)

constants are slightly different. In Fig. 3a, the two center lines are separated by 2.8 Hz (33.2–30.4 Hz). In Fig. 3b, both coupling constants are scaled up by a factor of 3, resulting in a splitting of $3 \times 2.8 = 8.4$ Hz for the center line. The main advantage of constant-time evolution is the possibility to unravel superimposed multilabeled signals. This simplifies the assignment, because the spectra look similar to those obtained for monolabeled and unlabeled samples.

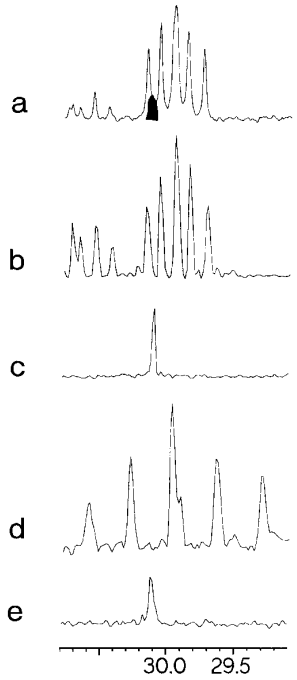

FIG. 5. (a) One-dimensional carbon signal of multilabeled Pro C3 superimposed with natural-abundance Val C3 (black). (b) Extracted row from the region-selective HSQC (Pro C3 signal). (c) Extracted row from the region-selective HSQC (Val C3 signal). (d and e) Respectively, the same as (b and c), but with *J* scaling by a factor of 3.

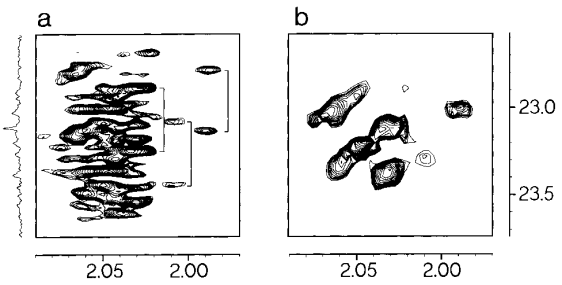

FIG. 6. Spectral sections of the *N*-acetyl CH_3 groups. On the left, the 1D carbon spectrum is shown. (a) The region-selective HSQC. All CH_3 groups show doublets in the carbon dimension with a coupling constant of 49 Hz. (b) The constant-time spectrum.

Figure 4 shows the Pro/Glx C3 region. In the CT spectrum (Fig. 4b), the Glu C3 signal is very well separated from the Gln/GSSG C3 signals. The latter are even identified as overlapping signals in the CT spectrum, while the region-selective HSQC consists of an insufficiently structured broad signal. Figure 4 also shows the superior signal separation in the 2D spectra compared to 1D carbon spectra. Figure 5 compares the extracted rows from the spectrum in Fig. 4 of the multilabeled proline C3 and the unlabeled natural abundance Val C3 signals with the 1D carbon signal. The two signals can be completely separated in the selective HSQC and the signals can be quantified.

The simultaneous excellent sensitivity and resolution is demonstrated in Fig. 6, where the region of the *N*-acetyl CH_3 groups is depicted. These groups experience the highest sensitivity improvement with respect to the 1D carbon spectrum (*14*) which is shown on the left. The doublet splitting in the carbon dimension (49 Hz) indicates doubly labeled acetyl groups and proves a *de novo* acetylation within the incubation time. At least 14 different $N-CO-CH_3$ groups can be distinguished.

The region-selective HSQC methods presented overcome the main disadvantage of inverse 2D spectroscopy, namely the poor resolution in the carbon dimension. The methods are now more versatile and useful for the analysis and quantification of ^{13}C multiplets. They offer superior signal separation and much better signal-to-noise ratios compared to 1D carbon spectroscopy and can be combined with *J* scaling, constant-time evolution, and TOCSY experiments.

REFERENCES

1. B. Künnecke, S. Cerdan, and J. Seelig, *NMR in Biomed.* **6,** 264–277 (1993).

2. A. Lapidot and A. Gopher, *J. Biol. Chem.* **269,** 27,198–27,208 (1994).

3. F. Chapa, F. Cruz, M. Moldes, P. Grühlke, B. de Mateo, M. J. Mate, and S. Cerdan, *Q. Magn. Reson. Biol.* **1,** 107–116 (1994).

4. S. S. Likhodii and S. C. Cunnane, *Magn. Reson. Med.* **34,** 803–813 (1995).

5. E. D. Lewandowski, C. Doumen, L. T. White, K. F. LaNoue, L. A. Damico, and X. Yu, *Magn. Reson. Med.* **35,** 149–154 (1996).

6. U. Flögel, W. Willker, J. Engelmann, T. Niendorf, and D. Leibfritz, *Dev. Neurosci.* **18,** 449–459 (1996).

7. W. Willker, D. Leibfritz, R. Kerssebaum, and W. Bermel, *J. Magn. Reson.* **31,** 287–292 (1993).

8. W. Willker, U. Flögel, and Dieter Leibfritz, *J. Magn. Reson. Anal.,* in press.

9. E. Kupce and R. Freeman, *J. Magn. Reson. A* **117,** 246–256 (1995).

10. L. E. Kay, P. Keifer, and T. Saarinen, *J. Am. Chem. Soc.* **114,** 10,663–10,665 (1992).

11. J. Schleucher, M. Schwendinger, M. Sattler, P. Schmidt, O. Schedletzky, S. J. Glaser, O. W. Sørensen, and C. Griesinger, *J. Biomol. NMR* **4,** 301–306 (1994).

12. L. Emsley and G. Bodenhausen, *Chem. Phys. Lett.* **165,** 469–476 (1990).

13. R. V. Hosur, *Prog. NMR Spectrosc.* **22,** 1–53 (1990).

14. W. Willker, J. Engelmann, A. Brand, and D. Leibfritz, *J. Magn. Reson. Anal.* **2,** 21–32 (1996).